

# Collective oscillations in quantum rings: a broken symmetry case

M. Valín-Rodríguez, A. Puente, and Ll. Serra

Departament de Física, Universitat de les Illes Balears, E-07071 Palma de Mallorca, Spain

24 march 2000

**Abstract.** We present calculations within density functional theory of the ground state and collective electronic oscillations in small two-dimensional quantum rings. No spatial symmetries are imposed to the solutions and, as in a recent contribution, a transition to a broken symmetry solution in the intrinsic reference frame for an increasingly narrow ring is found. The oscillations are addressed by using real-time simulation. Conspicuous effects of the broken symmetry solution on the spectra are pointed out.

**PACS.** 73.20.Dx Electron states in low dimensional structures – 78.20.Bh Theory, models and numerical simulation

## 1 Introduction

Quantum rings have attracted much interest in recent years. They constitute a clear example of the great technological advances in the fabrication of electronic nanostructures, which also include a rich variety of quantum dots. Theoretical studies of rings have addressed the appearance of the so called ‘persistent current’ as a function of an applied magnetic field, as well as the electronic structure and optical excitations within a fully microscopic approach for small rings [1,2,3]. On the other hand, semiclassical methods have been applied to larger rings [4], for which there exist experimental results in the mesoscopic domain [5]. These semiclassical methods have indeed provided a good description of the  $B$ -dispersion in the measured far-infrared collective excitations for large rings. At an intermediate theoretical level, microscopic density-functional calculations have been applied to describe rings containing around  $N \approx 10$  electrons [6,7]. An exciting prediction of these latter calculations is the transition for increasingly narrow rings (approaching the quasi-1d limit) to a state with broken rotational symmetry in the intrinsic reference frame containing a static spin-density wave (SDW). The fabrication of such rings, with a small number of electrons, is a very demanding challenge that only recently has been addressed by Lorke *et al.*, who reported measurements of the far infrared response of two electron rings [8,9].

All calculations of ring excitations for intermediate sizes ( $N \geq 10$ ), using either semiclassical methods or density-functional theory (DFT), have imposed circular symmetry to the system and, therefore, have not been able to signal the influence of the broken symmetry ground state on the spectra. In this paper we relax the symmetry condition on the ground and excited states of rings with the purpose to explore these effects within DFT. To this end we will use real time simulations of the collective density oscillations developed by two of us in the context of

quantum dots [10,11]. The paper is organized as follows: in Sec. II we consider the ring ground-state within our approach, focussing on the transition to the symmetry-broken ground state; in Sec. III we address the real time simulation of the charge and spin-density oscillations. Finally, the conclusions are drawn in Sec. IV.

## 2 DFT description of rings

In order to model two-dimensional (2d) quantum rings of varying widths we have used the model proposed by Reimann *et al.* [6] and consider a ring confining potential on the  $xy$  plane depending only on the radial distance  $r$ , such as

$$V^{(ext)}(r) = \frac{1}{2} \frac{\omega_0^2}{\delta} (r - R_0)^2. \quad (1)$$

In this expression  $R_0$  corresponds to the ring radius and we take  $\omega_0^2 = 1/r_s^3 N_p^{1/2}$ , with  $N_p$  and  $r_s$  parameters analogous to those giving for a circular quantum dot the number of positive charges and the Wigner-Seitz radius, respectively. The  $\delta$  parameter is introduced in order to model the radial thickness of the ring. As  $\delta$  decreases, the ring becomes thinner and thinner, approaching the quasi-1d limit.

We describe the electronic structure within the local-spin-density approximation of DFT. The reader is referred to Refs. [12,13] for details of the approach in the present context. The set of single-particle (sp) orbitals is obtained by selfconsistently solving the Kohn-Sham (KS) equations

$$\left[ -\frac{1}{2} \nabla^2 + V^{(ext)}(r) + V^{(H)}(\mathbf{r}) + V_{\eta}^{(xc)}(\mathbf{r}) \right] \varphi_{i\eta}(\mathbf{r}) = \varepsilon_{i\eta} \varphi_{i\eta}(\mathbf{r}), \quad (2)$$

where  $V^{(H)}$  and  $V_{\eta}^{(xc)}$  are respectively the Hartree and exchange-correlation potentials. The latter one is obtained

from the local energy density as

$$V_{\eta}^{(xc)} = \frac{\partial \mathcal{E}_{xc}(\rho, m)}{\partial \rho_{\eta}}, \quad (3)$$

In these expressions  $\eta = \uparrow, \downarrow$  labels the spin components while the spin densities are  $\rho_{\eta}(\mathbf{r}) = \sum_i |\varphi_{i\eta}(\mathbf{r})|^2$ . Total density and spin magnetization are given by  $\rho = \rho_{\uparrow} + \rho_{\downarrow}$  and  $m = \rho_{\uparrow} - \rho_{\downarrow}$ , respectively. Our exchange-correlation functional is based on the Tanatar-Ceperley results for the 2d electron gas [14] with the von Barth-Hedin interpolation for intermediate polarizations [15].

We emphasize here that our solution to Eq. (2) is not assuming *a priori* any symmetry for the orbitals  $\varphi(\mathbf{r})$ . The 2d plane is discretized into a uniform grid of points in Cartesian coordinates and the Laplacian operator is approximated by the corresponding finite differences (we have used typically 7 point formulas). The KS solutions are then obtained by iteratively applying the *imaginary-time-step* method. This technique is very robust although convergence may be rather slow in some cases. The lowest energy solution in each case is obtained by performing calculations with different starting points in order to assure that the result does not correspond to a local minimum representing an excited state of the system.

### 2.1 Circular rings

Figure 1 shows the density and magnetization for a ring with [16]  $R_0 = 8$ , containing  $N = 10$  electrons and for two values of the width  $\delta$ . The wide one ( $\delta = 2$ ) has perfect circular symmetry and its magnetization vanishes. On the contrary, the narrow one ( $\delta = 0.08$ ) presents a modulation in charge density, a charge density wave (CDW), and spin polarization of antiferromagnetic type, with alternate orientations of spin up and down (a SDW). This dramatic change of behaviour is associated with the increase of the radial confinement and agrees with the findings of Ref. [6]. We compare in Fig. 2 the energy of the unrestricted solution to Eq. (2) with that obtained with the constraint of circular symmetry, i.e., by solving only the radial KS equation as in Ref. [7]. Also shown in Fig. 2 is the ratio of maximum magnetization to maximum density and the amplitude of the CDW. Panels (b) and (c) show that the transition is rather abrupt with the value of  $\delta$ , although the energy (panel (a)) is smoothly changing. Nevertheless, the energy trend is very clear and manifests the gain in binding energy with the formation of CDW's and SDW's.

Although some controversy has existed in the quantum dot community [12,17,18], the formation of broken-symmetry solutions as those displayed by mean-field theories is a well known phenomenon in nuclear physics [19] and in atomic physics [20]. It has been recently discussed in the context of 2d quantum dots by Yannouleas and Landman [18] and by Koskinen et al [12,21]. It has been shown that the mean field solution corresponds to the intrinsic structure of the system although the full exact solution in the laboratory frame preserves the symmetry because of an underlying degeneracy. This is convincingly shown by

comparing internal structure properties of the exact solution, such as the conditional pair probability, with the mean field result [18]. Another strong evidence of the internal symmetry breaking is given by the comparison of the low lying states with the roto-vibrational states of the structure formed by the localized electrons [18,21]. Quantum rings constitute indeed a very good scenario for this behaviour since, as shown in Figs. 1 and 2, they exhibit strong breaking of the circular symmetry. A critical comparison of the mean field solution with the exact one for two-electron quantum rings will be presented in a future publication.

The broken-symmetry solution is accompanied by a strong change in the sp level scheme. While the circular structure is characterized by shells, with closings at electron numbers of 2, 6, 10, 14 and a small sensitivity on the width  $\delta$ , the formation of SDW's and CDW's leads to a bunching of the occupied levels and the formation of a relatively large energy gap at the Fermi level. This behaviour is shown in panel (d) of Fig. 2.

### 2.2 Elliptic rings

Deformed rings can be simulated by using an elliptic contour for  $R_0(\theta)$  of the type

$$R_0(\theta) = a \left( \cos^2 \theta + \frac{1}{\beta^2} \sin^2 \theta \right)^{-\frac{1}{2}}, \quad (4)$$

where  $a$  is the major axis of the ellipse,  $\beta$  gives the ratio of minor to major axis and  $\theta$  is the polar angle. In order to compare with the circular rings of the preceding subsection we have taken elliptic rings with the same perimeter and have considered two deformations, namely  $\beta = 0.75$  and  $\beta = 0.5$ , corresponding to medium and large ring deformation, respectively.

One of the most striking findings in elliptic rings is the appearance of the broken-symmetry solution along the ring contour *for increasing deformation*, at fixed width. This happens even for wide rings although the wave structure is more clearly marked in the narrow ones (Fig. 3). Another behaviour which is apparent in Fig. 3 is the formation of charge concentrations at the ends of the long axis. These are attributed to *end states* similar to those found in finite wires [6]. In broad rings, the formation of end states appears abruptly after a minimum deformation is reached. For instance, at  $\delta = 2$  and  $\beta = 0.75$  no evidence is yet found of their formation.

## 3 Time dependent spin and charge density oscillations

The analysis of excited states is often made by invoking perturbation theory for an external probing field. The feasibility of this approach usually relies on the symmetries of the system, which greatly simplify the treatment. For instance, in circular dots one can take density oscillations

of the type  $\delta\rho_\eta(\mathbf{r})e^{im\theta}$ , i.e., a radial function times a multipolar field, and then reduce the equations to the radial parts. In the present context the possibility of having a broken symmetry ground state forbids this approach.

A suitable alternative to perturbation theory is to study the density oscillations by using real-time simulations. This is particularly well adapted to DFT and leads to its time-dependent generalization (TDDFT). The simplest version of this scheme is the adiabatic-local-density approximation, which uses the energy functional of the ground state to explore small amplitude oscillations around it. This is one of the simplest versions of TDDFT and yet it is quite robust and satisfies known exact properties as the energy weighted sum rule and the generalized harmonic-potential theorem [22, 23]. We will use it to calculate the ring spin-density oscillations.

The time-dependent Schrödinger equations can be written

$$i\frac{\partial}{\partial t}\varphi_{i\eta}(\mathbf{r}, t) = h_\eta[\rho, m]\varphi_{i\eta}(\mathbf{r}, t), \quad (5)$$

where the KS single-particle Hamiltonian  $h_\eta[\rho, m]$  is given by the square bracket in Eq. (2), whose stationary solution was found in the preceding Section. Here we will perform an initial (at  $t = 0$ ) perturbation of the wave functions

$$\varphi_{i\eta}(\mathbf{r}, 0) = \mathcal{P}\varphi_{i\eta}(\mathbf{r}), \quad (6)$$

and track the time evolution through Eq. (5). Technical details of the integration method, as well as of the analysis of the dipole signals  $\langle\mathbf{r}\rangle_\eta$  which allow to extract the excitation spectrum can be found in Refs. [10, 11].

We will distinguish three different types of excitation modes, two of them depending on the initial perturbation  $\mathcal{P}$  and another one corresponding to a theoretical model in which the electrons are not interacting. Namely: *density modes* associated with an initial rigid displacement of the total density; *spin modes* for which at  $t = 0$  the spin densities are rigidly shifted in opposite directions; and *free modes* for which the sp Hamiltonian is kept fixed to the stationary densities, i.e.,  $h_\eta[\rho, m] \approx h_\eta[\rho_0, m_0]$ . The free oscillations, also known as sp modes, are equally excited by shifting either the total density or the spin densities.

### 3.1 circular rings

Figure 4 shows the free, density and spin spectra for the broad ring with  $N = 10$  and  $\delta = 2$ . As known from other calculations [4, 7] the spectrum is roughly divided in two regions in the sp model which are then shifted by the interaction in the density and spin channels. The lower region contains a single peak while the higher one exhibits an important fragmentation. The density response is characterized by the blue shift from the sp peaks while the spin response exhibits a shift to lower energy. The residual interaction is also quite effective in enhancing one peak above the others in the high energy region. The peak that collects the strength is then associated to the more collective excitation. These features can be considered standard in finite Fermi systems with a repulsive interaction in the

density channel and an attractive one for the spin channel. Indeed, a similar behaviour has been found in quantum dots. Figure 4 also shows the corresponding spectra obtained by using the circularly constrained solution in the perturbative random-phase approximation (RPA) [7]. It is obvious that both results are equivalent, as one would expect since the ground state has circular symmetry. We attribute the minor differences to the quite different techniques that have been used in the two cases. It is worth to notice that the real time method is much more demanding computationally and that very fine details of the spectrum are harder to describe, such as very low intensity peaks, or the resolution of two closely lying excitations.

The results for the narrow ring ( $\delta = 0.08$ ) are shown in Fig 5. Qualitative differences appear with respect to the preceding ring and, most important, with respect to the circularly constrained solution. They must be attributed to the symmetry breaking ground state of this ring. The separation of high and low energy region is now clearer, with an important gap between both. The most striking result comes from the comparison of the low energy peaks with the circularly constrained solution. First we notice that the full solution in this energy region yields a density response which is very close to, but just below, the sp peaks and overlaps with some excitations of the spin response. In the circularly constrained calculation the density response is above the sp one and, furthermore, the spin peak lies at an essentially vanishing energy. The different behaviour is indicating that the symmetry breaking is giving stability to the ring, which would otherwise become unstable against spin oscillations. This is in agreement with the appearance of an energy gap in the sp energies associated to the symmetry breaking, mentioned in Sec. II.

The high energy region is associated to a locally radial oscillation in the ring, and thus similar to the oscillation in a one dimensional oscillator. This is confirmed by the similarity of the energy with the radial curvature at the minimum given by  $\omega_0/\sqrt{\delta}$  that, by the well known generalized Kohn's theorem, is the only allowed energy for rigid density oscillations of dipole type in parabolic confinement [24]. On the other hand, the low energy region is associated with oscillations locally tangential to the ring. Within this interpretation, the fact that the density and spin tangential modes are close in energy and essentially overlap with the sp excitations can be understood as a signature of a 1-dimensional Luttinger liquid [25], for which the lowest excitations are not the sp but the collective ones.

In the symmetry broken ground state there is also a possibility to excite pure tangential modes by means of a twist of the two spin densities in opposite directions. These *exotic* modes were proposed recently in the context of quantum dots [10]. It is obvious that pure tangential modes can not exist in circularly symmetric rings since a twist of spin densities does not change the energy. However, in a symmetry broken state a restoring force appears because of the distortion of the spin-density wave. The associated oscillation energy is easily obtained by analyzing

the time dependence of the orbital currents  $\langle \sum_i \ell_i^{(z)} \sigma_i^{(z)} \rangle$  that appear after an initial spin twist.

Figure 6 shows the spin twist spectrum for the narrow ring with 10 electrons. We observe that the peaks are in the same region as the low energy dipole excitations, which is proving that the latter ones are indeed of tangential nature. Both free and interacting spectra are characterized by a rather regular energy spacing, after an initial gap. We attribute this to the parabolicity of the potential in the tangential direction for points close to the local minima.

### 3.2 Elliptic rings

The systematics with deformation is very similar to that discussed for the circular case, with the additional result that both dipole energy regions are now more fragmented. Figure 7 shows the corresponding spectra for a strongly deformed ring  $\beta = 0.5$  with thicknesses given by  $\delta = 2$  and  $\delta = 0.08$ . This fragmentation is more regular in the wide rings, with a doubling of high and low energy peaks by the same energy separation. In the narrow ring the relative fragmentation is lower with respect to the separation of high and low energy regions which is in agreement with the previously mentioned transverse and longitudinal character of both regions.

## 4 Conclusions

The ground state and oscillations of quantum rings have been discussed within density-functional theory relaxing the constraint of circular symmetry of the electronic density. A transition to a broken symmetry ground state with static charge and spin density waves has been found for increasingly narrow rings, in agreement with previous results. The energy gain with respect to the circularly constraint solution, the amplitude of charge and spin-density wave as well as the sp level scheme have been discussed as a function of ring width. The transition to a wave structure along the ring contour has also been obtained in elliptic rings for increasing deformations. In this case, there also appear charge concentrations at the long axis ends indicating the formation of end states similar to those obtained in finite quantum wires.

Signatures of the broken symmetry ground state on the collective oscillation energies have been searched for in the dipole spin and density oscillations. We have shown that the broken symmetry is accompanied by an overlap of the density and spin response peaks in the low energy region corresponding to tangential oscillations. At the same time, the low lying sp excitations are at a slightly higher energy, which is indicating a quasi 1d behaviour similar to that of Luttinger liquids. The energy of these excitations is close to the gap associated to the broken symmetry. It has also been shown that the broken symmetry gives stability to the ring, which would otherwise become unstable against spin dipole oscillations. The oscillations in the radial direction are located at higher energy, close to the radial curvature of the parabola as indicated by the generalized

Kohn's theorem. The separation between high and low energy regions increases as the ring width decreases.

Pure tangential modes in rings with broken symmetry, associated to a twist of the spin densities have been discussed and it has been shown that their energy is close to the low dipole peaks. This supports the interpretation of this dipole excitations. Besides, we have shown that the more exotic spin-twist modes are regularly spaced in energy because of a high degree of harmonicity of the potential. Finally, the dipole oscillations in elliptic rings have been obtained and their fragmentation depending of the ring width has been shown.

Further work is necessary in order to analyze in detail the convergence to the strict 1d limit, for very narrow rings, and how the peculiarities of a Luttinger liquid such as power-law (as opposite to long range) order in the SDW correlation function and spin-charge separation [25] may manifest in a finite size system.

## 5 Acknowledgements

M.V.-R. gratefully acknowledges support by the Consell de Mallorca-UIB. This work was performed under grant No. PB98-0124.

## References

1. T. Chakraborty and P. Pietiläinen, Phys. Rev. B **50**, 8460 (1994); and references therein.
2. V. Halonen, P. Pietiläinen and T. Chakraborty, Europhys. Lett. **33**, 377 (1996).
3. L. Wendler *et al.*, Phys. Rev. B **54**, 4794 (1996).
4. E. Zaremba, Phys. Rev. B **53**, 10512 (1996)
5. C. Dahl, J. P. Kothaus, H. Nickel, and W. Schlapp, Phys. Rev. B **48**, 15480 (1993)
6. S. M. Reimann, M. Koskinen and M. Manninen, Phys. Rev. B **59**, 1613 (1999)
7. A. Emperador *et al.*, Phys. Rev. B **59**, 15301 (1999)
8. A. Lorke *et al.*, LANL preprint cond-mat/9908263.
9. A. Lorke and R. J. Luyken, Physica B **256**, 424 (1998).
10. A. Puente and Ll. Serra, Phys. Rev. Lett. **83**, 3266 (1999).
11. Ll. Serra, A. Puente and E. Lipparini, Phys. Rev. B **60**, 13966 (1999).
12. M. Koskinen, M. Manninen, and S. M. Reimann, Phys. Rev. Lett. **79**, 1389 (1997).
13. M. Pi *et al.*, Phys. Rev. B **57**, 14783 (1998).
14. B. Tanatar and D. M. Ceperley, Phys. Rev. B **39**, 5005 (1989).
15. U. von Barth and L. Hedin, J. Phys. C **5**, 1629 (1972).
16. All numerical values, unless stated otherwise, are given in effective units, for which  $\hbar = m^* = e^2/\epsilon = 1$ . Then, the energy unit is  $H^* = 12$  meV and the length unit  $a_0^* = 98$  Å.
17. K. Hirose and N. S. Wingreen, Phys. Rev. B **59**, 4604 (1999).
18. C. Yannouleas and U. Landman, Phys. Rev. Lett. **82**, 5325 (1999); LANL preprint cond-mat/0002364; cond-mat/0003245.
19. P. Ring and P. Schuck, *The nuclear many body problem*, (Springer-Verlag, NY, 1990).

20. R. S. Berry, Contemporary Phys. **30**, 1 (1989).
21. M. Koskinen, M. Manninen, B. Mottelson and S. M. Reimann, LANL preprint cond-mat/0004095.
22. J. F. Dobson, Phys. Rev. Lett. **73**, 2244 (1994).
23. E. Lipparini *et al.*, Phys. Rev. B **56**, 12375 (1997).
24. P. A. Maksym and T. Chakraborty, Phys. Rev. Lett. **65**, 108 (1990).
25. F. D. M. Haldane, J. Phys. C **14**, 2585 (1981); for a review, see J. Voit, Rep. Prog. Phys. **57**, 977 (1994).

**Fig. 1.** Results for a ring with  $N = 10$  electrons,  $R_0 = 8$  and parameters  $N_p = 10$ ,  $r_s = 1.51$  (see text). From left to right the density for a ring width  $\delta = 2$ , the density for  $\delta = 0.08$  and the magnetization for  $\delta = 0.08$  are shown, respectively.

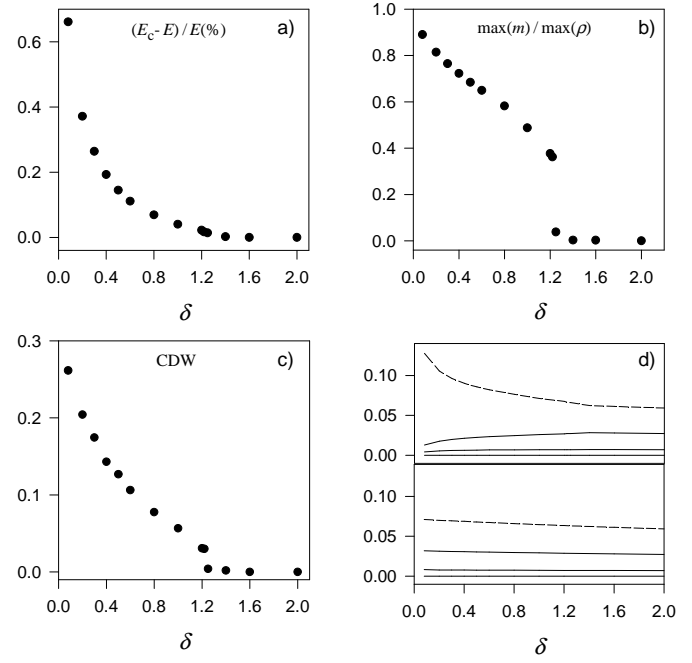


**Fig. 2.** Evolution with  $\delta$  of several properties for the same ring of Fig. 1. Panel (a) shows  $(E_c - E)/E$  in percentage, where  $E_c$  is the energy of the circularly constrained solution while  $E$  is that of the full solution to Eq. (2). Panel (b) shows the evolution of the ratio of maximum magnetization over maximum density. Panel (c) displays the amplitude of the charge-density wave and panel (d) shows the evolution of the energy level scheme referred to the lowest sp orbital. In this latter panel, occupied levels are plotted with solid lines while the first unoccupied one is shown with a dashed line.

**Fig. 3.** Density and magnetization for elliptic rings with 10 electrons and  $\delta = 2$ . For  $\beta = 0.75$  only the density is shown, since the magnetization vanishes, while for  $\beta = 0.5$  both density and magnetization are displayed.

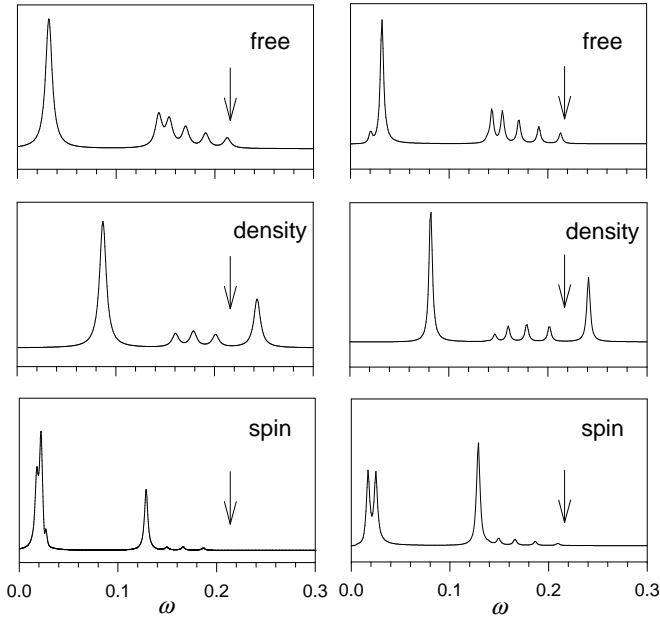


**Fig. 4.** Dipole oscillation spectra in the free, density and spin channels for the circular ring with  $N = 10$  and  $\delta = 2$ . The left panels correspond to the unrestricted solution while the right panels show the circularly constrained one. The arrow shows the value  $\omega_0/\sqrt{\delta}$ , that gives the curvature of the radial parabola at the minimum.

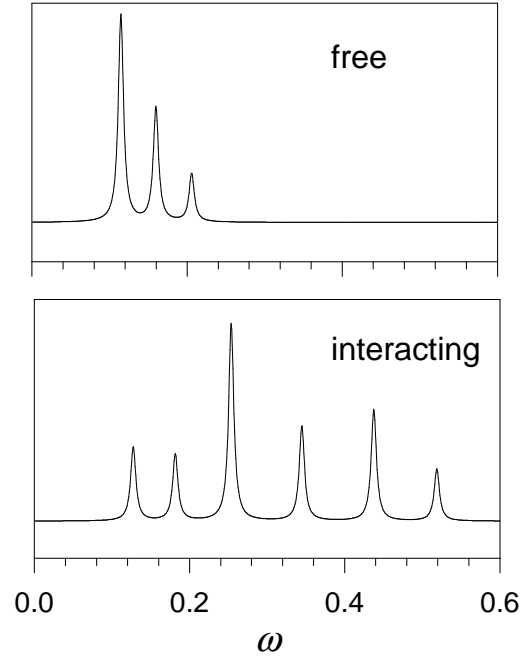


**Fig. 6.** Spin twist spectra for the narrow circular ring in the free and interacting channels.

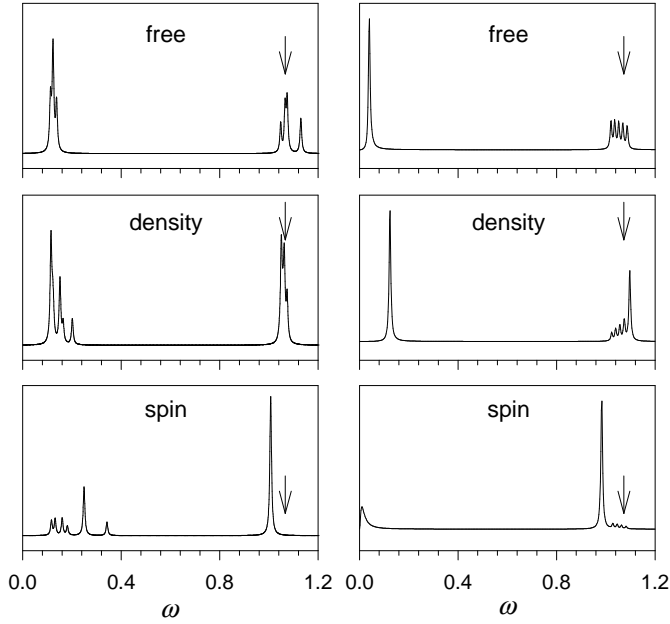


**Fig. 5.** Same as Fig. 4 but for  $\delta = 0.08$ .

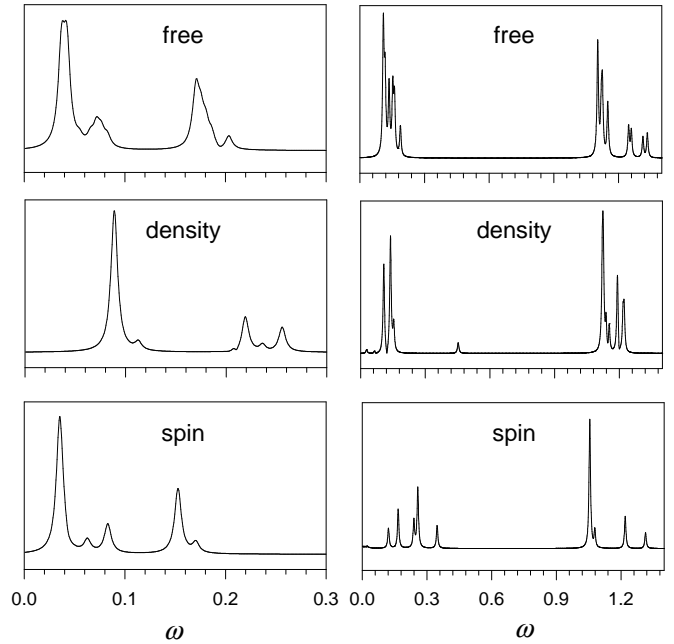


**Fig. 7.** Same as Fig. 4 for a deformed ring with  $\beta = 0.5$ . Left panels correspond to  $\delta = 2$  and right ones to  $\delta = 0.08$ .

This figure "fig1.gif" is available in "gif" format from:

<http://arxiv.org/ps/cond-mat/0006194v1>

This figure "fig3.gif" is available in "gif" format from:

<http://arxiv.org/ps/cond-mat/0006194v1>